

Fe₃O₄ Nanoparticles from FeSiAl Alloy of Spent Printed Circuit Boards and its Application in Dye Degradation

Dinesh Patil^a, M. B. Sridhara^{a,*}, J. Manjanna^{a,*}, Sandip Sabale^b

a) Department of Chemistry, Rani Channamm a University, Belagavi 591 156, Karnataka, India

b) P.G. Department of Chemistry, Jaysingpur College, Jaysingpur, 416 101, Maharashtra, India

Received 22 December 2022; received in revised form 23 March 2023; accepted 9 May 2023 (DOI: 10.30495/IJC.2023.1975703.1985)

ABSTRACT

Fe is an important element, used in soft magnetic materials (cores) in electrical and electronic devices and its concentration in e-waste is high. Thus, this study is aimed to recover Fe from the soft magnetic FeSiAl cores of spent printed circuit boards (PCBs). Here, the Fe-rich FeSiAl cores were identified, separated manually, and subjected to dissolution in citric acid (100 mM) and ascorbic acid (10 mM) mixture at 80 °C. The dissolved Fe was selectively precipitated as Fe₃O₄ using 20% NaOH in an N₂ atmosphere at 90 °C for about 60 min. The obtained Fe₃O₄ shows ferromagnetic behavior with 30 emu/g saturation magnetization at 300 K. The BET surface area of Fe₃O₄ NPs was found to be 71.656 m² g⁻¹. Furthermore, the Fe₃O₄ NPs were utilized for methylene blue degradation with H₂O₂ in visible light irradiation. At optimum conditions, such as 10 ppm MB solution, 0.1 mL H₂O₂, and an S:L ratio of 0.05 g/L about 100% degradation was achieved in about 45 min under visible light irradiation and the correlated rate constant is 0.084 min⁻¹. We believe that the synthesis of value-added compounds directly from the dissolution medium is an environmentally benign step toward resource recycling.

Keywords: Citric acid and ascorbic acid; Fe₃O₄; Spent PCBs; Soft magnetic FeSiAl cores.

1. Introduction

The soft magnetic materials are easily magnetized and demagnetized and possess coercive field strength of 40 A/m [1, 2]. Owing to the unique properties such as magnetic and thermal isotropy, high magnetic permeability, high remanent magnetization, high resistivity, large anisotropy constant, low coercivity, and high Curie temperature, these materials are used in various devices like generators, transformers, inductors, motors, etc [1, 3]. The fast-rising information technology industry produces advanced electric and electronic equipment (EEE) like smartphones, televisions, computers, etc. at an increasing rate [4]. This development in technology increases the consumption of EEE devices, which in turn increases the utilization of primary resources. The fast expansion of the information technology industry and increasing demand for EEE are driving the ever-increasing

generation of *E-waste* [4]. Industries such as textile, paper, leather, printing, paint, coating, and papermaking utilize various dyes [5, 6]. Over 1 lakh types of dyes are listed with annual pollution of about 7×10^5 tons of which textile industries consume around 36,000 tons each year. According to the World Bank around 20% of dye, pollution comes from dyeing and textile industries [5, 6, 7]. In the year 2020, the world dyes market was around US\$ 7.9 billion, which is projected to grow to US\$ 10.6 billion by 2027 [8]. According to studies, the staining of cotton required a large amount of water and it was calculated that about 15 liters of water are required to tint 1 kg of textile [9]. Methylene blue (MB) is a vital member of the thiazine class of dyes, which is usually utilized by the textile industry. The discharge of colored industrial wastewater into natural water bodies without any pretreatment presents an eco-toxic hazard and introduces the possible danger of bioaccumulation and it was reported to be cancer-causing and mutagenic [10]. In addition, it causes nausea, vomiting, diarrhea, and difficulty breathing upon consumption [11].

*Corresponding author:

E-mail address: sridhara.mb@gmail.com (M. B. Sridhara);
jmanjanna@rediffmail.com (J. Manjanna)

Therefore, the treatment of colored water before released into the environment is of great concern.

Degradation of dyes using a semiconductor-based catalyst in the presence of visible light is an advanced oxidation process (AOP) [12]. Fe_3O_4 is a low-cost, narrow-band gap semiconductor with visible light sensitivity. To improve the catalytic activity of Fe_3O_4 NPs, researchers have reported the preparation of Fe_3O_4 composites such as $\text{Fe}_3\text{O}_4/\text{FeMnO}_x$ core/shell NPs [13], GO- Fe_3O_4 [14], G/ Fe_3O_4 [15], g- $\text{C}_3\text{N}_4/\alpha\text{-Fe}_2\text{O}_3/\text{Fe}_3\text{O}_4$ [16], RGO/ Fe_3O_4 [17], $\text{Fe}_3\text{O}_4/\text{GO}$ [18], ZnO- Fe_3O_4 [5] and so on.

The EEE is the secondary source for a number of vital metals. Various reports were available on the dissolution of spent PCBs, followed by the recovery of metals using mineral acids. However, in this study mixture of mild organic acids was used for FeSiAl alloy dissolution from spent PCBs. The Fe_3O_4 NPs were synthesized directly from the FeSiAl alloy dissolution mixture without adding any capping agent. Here, the leaching agents such as citric acid and ascorbic acid act as chelating agents, which stabilizes the dissolved Fe. In addition, the citric acid and ascorbic acid controlled the size of synthesized Fe_3O_4 in the nano regime. Furthermore, the recovered Fe_3O_4 NPs were utilized for MB degradation under visible light irradiation.

2. Experimental

Spent PCBs was collected from a local market of Belagavi, Karnataka. The citric acid (99%) (CA), and ascorbic acid (99%) (AA) were used as leaching agents in FeSiAl dissolution. The dissolved Fe was estimated using chemicals such as $\text{NH}_2\text{OH HCl}$ (98%) as a reducing agent for the conversion of Fe^{3+} to Fe^{2+} . 1,10-phenanthroline (99%) as a complexing agent, and a mixture of sodium acetate (98%) and acetic acid (99.5%) as a buffer. NaOH (98%) was used as a precipitant.

2.1. Dissolution of FeSiAl alloy

The FeSiAl alloy cores were manually separated from the spent PCBs and ground to a fine powder using mortar and pestle. The dissolution of powdered FeSiAl alloy material was performed in the presence of a CA and AA mixture [19]. Exactly, 1 g of FeSiAl has dissolved in 1000 mL of 100 mM CA and 10 mM AA mixture at 80 °C, pH = 2 in about 240 min. During the dissolution reaction, the reaction solution was collected periodically and estimated for Fe by an o-phenanthroline method at λ_{max} 510 nm [20].

2.2. Recovery of dissolved Fe as Fe_3O_4

The Fe_3O_4 was recovered from Fe dissolved solution. To the Fe dissolve solution, 20% NaOH solution was added dropwise till pH reaches 10 at 90 °C. The inert condition was maintained throughout the synthesis by purging N_2 gas. After the formation of a black precipitate, the solution was kept stirred for 60 min. Then, the precipitate was separated by membrane filtration, washed with distilled water and ethanol followed by vacuum drying at room temperature (25-28 °C). The black color magnetic powdered compound was stored in a vacuum desiccator at room temperature.

2.3. Degradation of MB dye

Degradation of MB was carried out through the photo-Fenton process in a photochemical reactor using a visible lamp (250 W) as a source of irradiation. During the degradation reaction, MB dye (5, 10, and 15 ppm) and Fe_3O_4 NPs (0.025, 0.05, and 0.075 g) were agitated with H_2O_2 (0.07, 0.1, 0.3, and 0.5 mL) in the presence of visible light [19]. The progress in the degradation reaction was monitored by a periodic collection of the reaction mixture using a UV-Vis spectrophotometer. Then, from the absorbance value at $\lambda_{\text{max}} = 664$ nm, the percentage of degraded MB was estimated.

3. Results and Discussion

3.1. Characterization of FeSiAl alloy

Fig. 1 shows the XRD pattern of FeSiAl alloy. All three distinct peaks at $2\theta = 44.6^\circ$, 65.1° , and 82.5° correspond to (110), (200), and (211) planes, respectively. The XRD pattern given here is very well matched with the reported patterns for FeSiAl alloy with bcc structure (JCPDS card no. 65-4899) [21-23]. Further, the elemental composition was confirmed from EDX data (**Fig. 2**), which shows the presence of elements Fe, Si, and Al with wt. % 96.8, 0.5, and 0.3, respectively [19].

3.2. Characterization of recovered product Fe_3O_4

Fig. 3a shows the XRD pattern of the recovered product (Fe_3O_4) from the FeSiAl dissolved solution of spent PCB. All the diffraction peaks were matched well with the cubic structure of Fe_3O_4 (JCPDS No. 00-003-0863) [24, 25]. The diffraction peaks at $2\theta = 30.1^\circ$, 35.5° , 43.2° , 53.6° , 57.1° , 62.6° , and 74.5° correspond to (200), (311), (400), (422), (511), (440), and (533) planes respectively. The Inset of **Fig. 3a** shows the FTIR spectra of Fe_3O_4 . Here, a significant peak was observed at 574 cm^{-1} corresponding to the stretching vibration of Fe-O [26]. The strong absorption bands at 3450 cm^{-1} and 1639 cm^{-1} were assigned to the OH stretching and bending vibration, respectively. The formation of Fe_3O_4

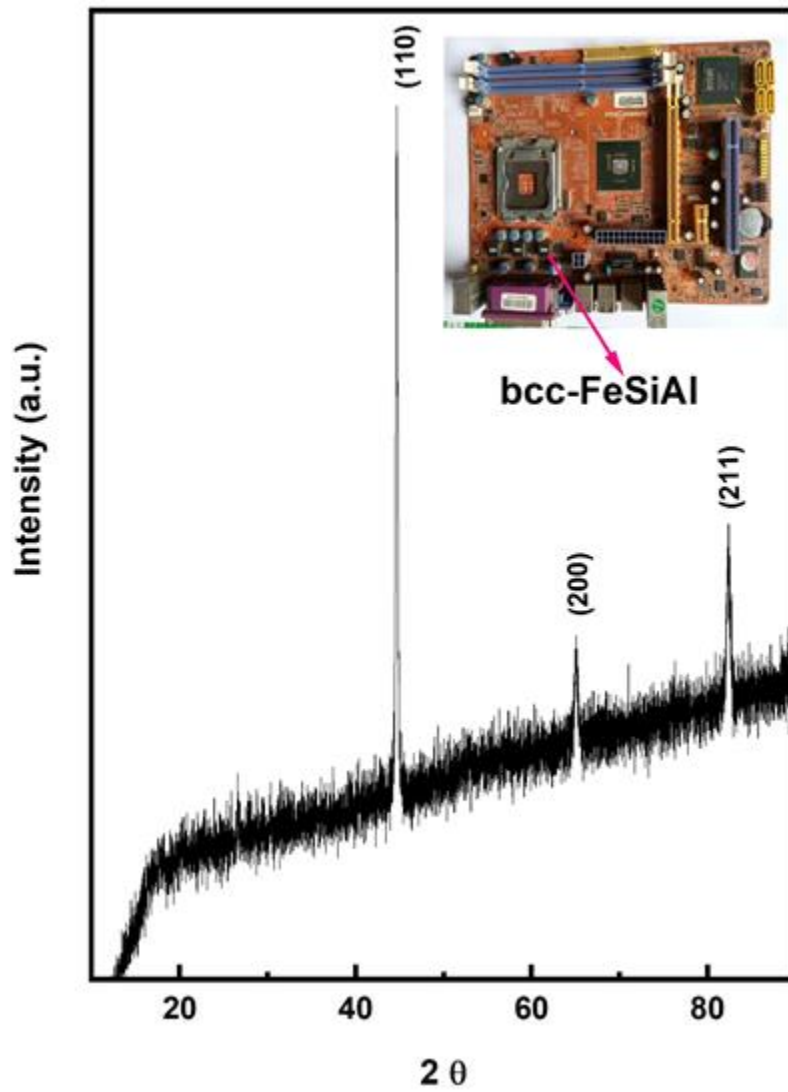


Fig. 1. Powder XRD pattern of soft magnetic FeSiAl alloy material collected from spent PCBs.

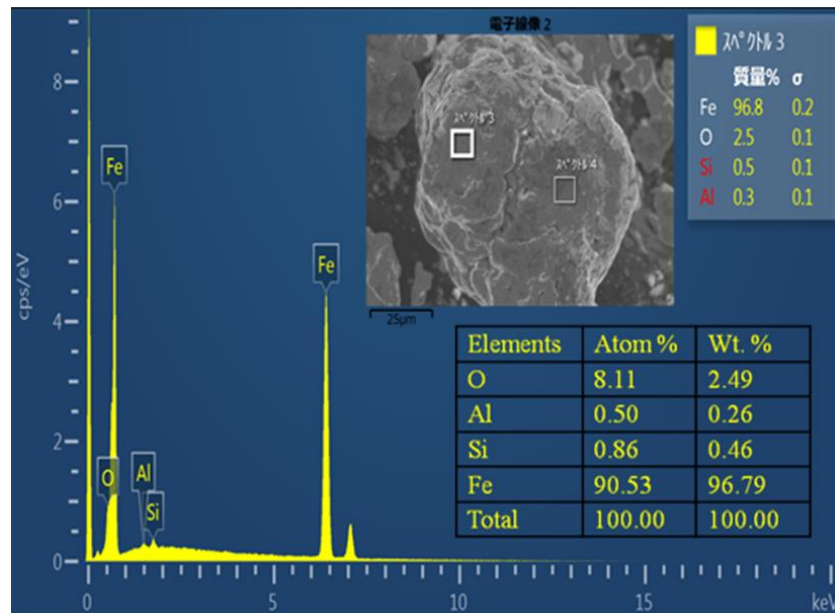


Fig. 2. EDX of soft magnetic FeSiAl alloy.

was also confirmed by the chemical method (i.e., o-phenanthroline method) [20] by calculating the amount of Fe^{2+} and Fe-total in the recovered Fe_3O_4 .

Scherrer's equation 1 was used to estimate the average crystallite size of Fe_3O_4 NPs.

$$D = \frac{0.9\lambda}{d\cos\theta} \quad (1)$$

Where D is the average crystallite size of Fe_3O_4 NPs in nm, 0.9 is the crystallite shape constant, λ represents the wavelength of the incident X-ray radiation (0.154 nm), β (radians) is the full width at half maximum of the peak in radians, and θ stands for the Bragg's angle of diffraction [23, 27-29]. The crystallite size of Fe_3O_4 NPs was calculated using equation 1 and it is found to be ~ 20 nm.

The magnetic measurement of recovered Fe_3O_4 was performed using a SQUID magnetometer at 300 K with a maximum applied field of ± 50 kOe. The particles were dispersed and fixed in an epoxy resin to eliminate the effects of interparticle interactions and their movement on magnetic properties. **Fig. 3b** shows the magnetization hysteresis of Fe_3O_4 at 300 K. The Fe_3O_4 shows a strong ferromagnetic property as evident from

the magnetic hysteresis loop (**Fig. 3b**). The saturation magnetization (M_s), 30 emu/g, remanence magnetization (M_r), 1.32 emu/g, and coercive field (H_c), 12 Oe are determined from the MH loop.

Fig. 4 depicts the FESEM-EDX images of recovered Fe_3O_4 . The FESEM images confirm that the obtained Fe_3O_4 is in the nano regime. The particles are agglomerated and are flat and irregular in shape. The EDX image shows the presence of Fe, 27.60 mass %, O, 33, and C, 38.72 mass %. A negligible amount of Na, 0.67 mass % impurity was observed in the recovered Fe_3O_4 .

The BET surface area and pore size distributions of Fe_3O_4 NPs were determined by nitrogen adsorption/desorption isotherm. As shown in **Fig. 5**, the Fe_3O_4 NPs exhibit an H3 type of hysteresis loop [30]. The BET surface area was found to be $71.656 \text{ m}^2 \text{ g}^{-1}$. The pore size distribution was determined by the BJH method using desorption isotherm. The total pore volume and mean pore diameter are found to be $0.3897 \text{ cm}^3 \text{ g}^{-1}$ and 21.756 nm, respectively. The high BET surface area and porosity of Fe_3O_4 NPs increase the active sites, which leads to high photocatalytic activity.

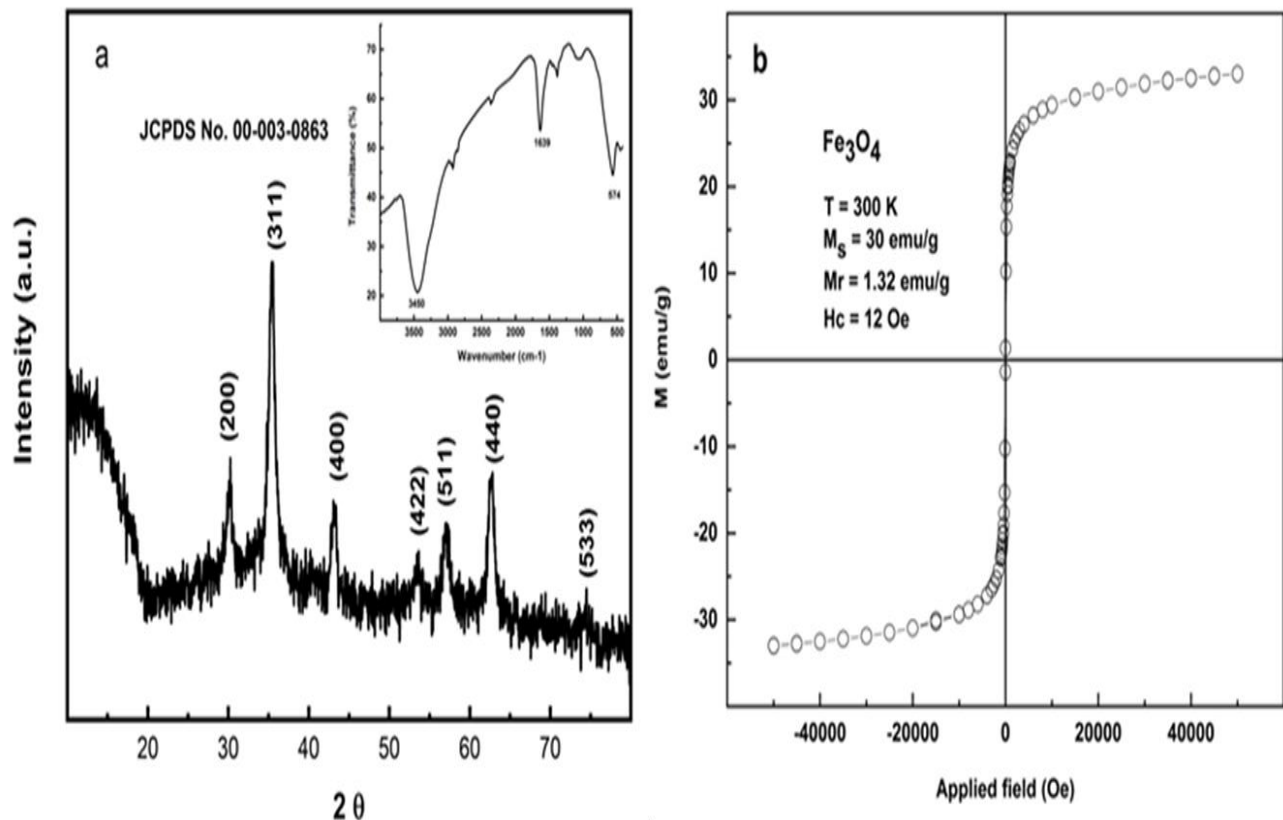


Fig. 3. a) XRD pattern of recovered Fe_3O_4 from FeSiAl dissolved solution (Inset shows the FTIR spectrum) and b) Magnetic hysteresis loop of Fe_3O_4 NPs at 300 K.

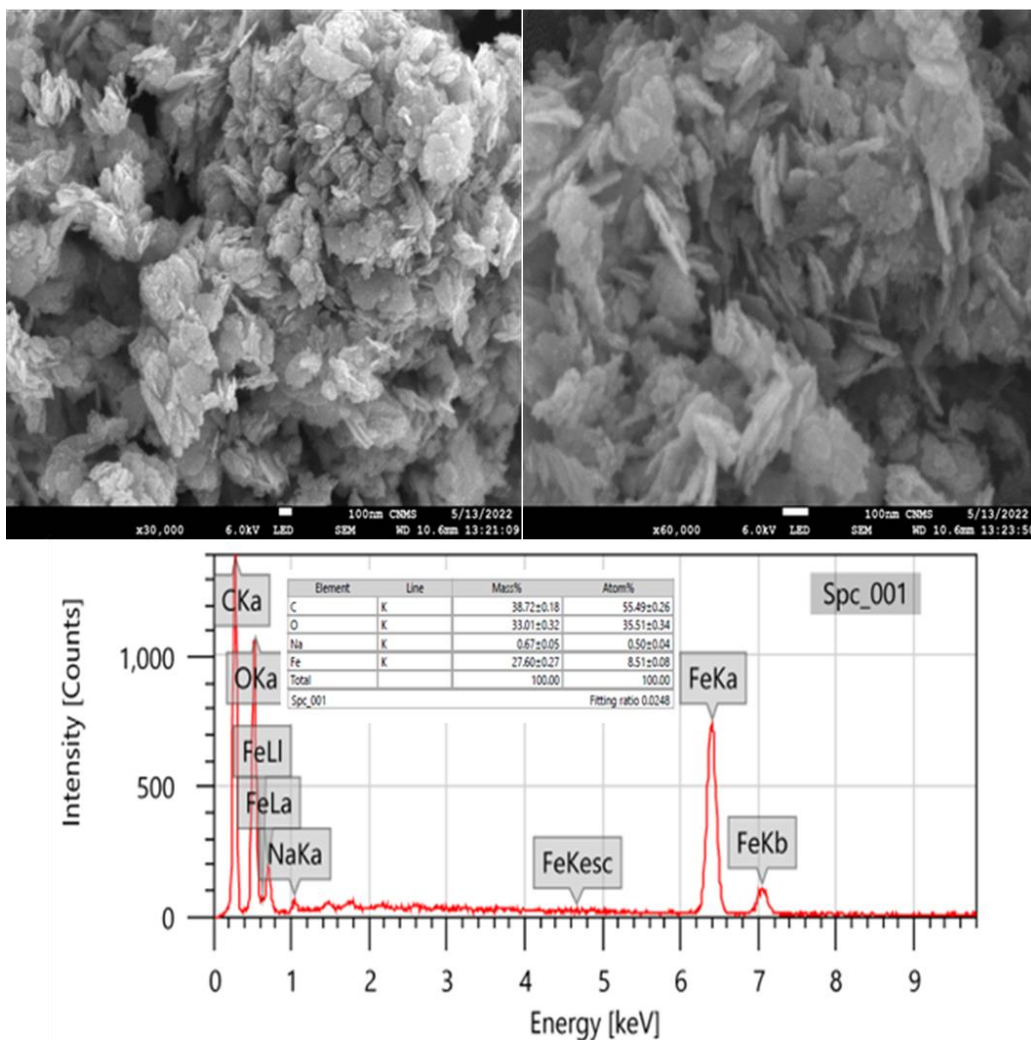


Fig. 4. FESEM-EDX images of recovered Fe₃O₄.

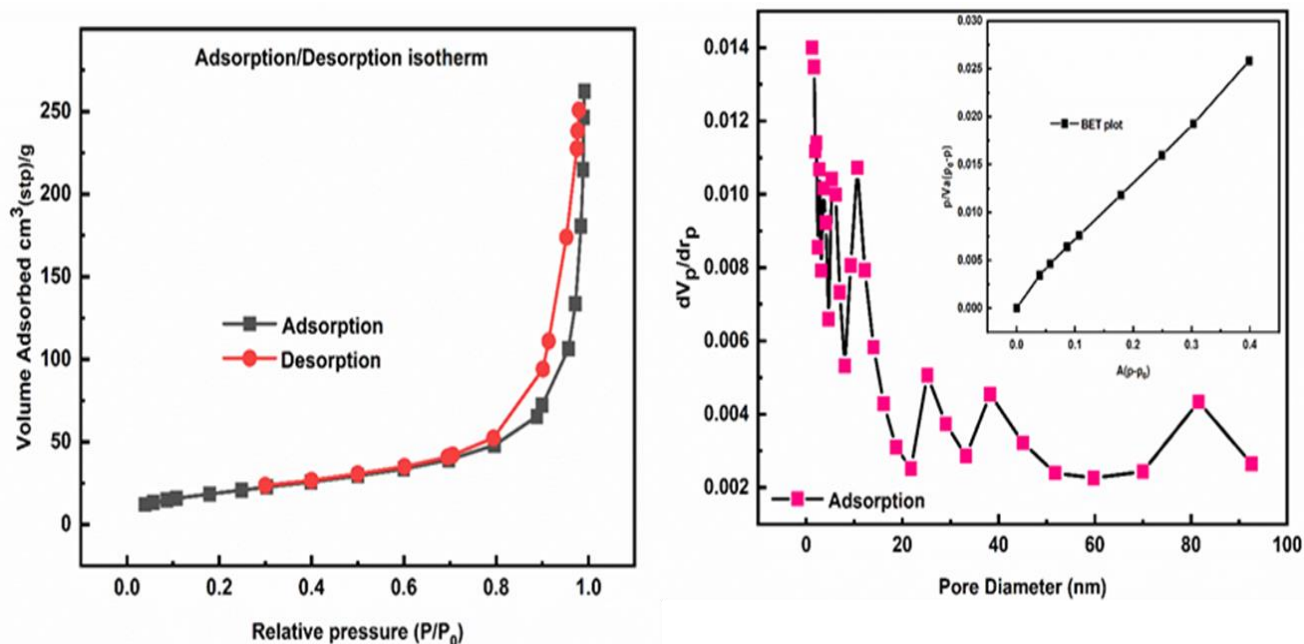
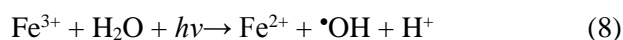
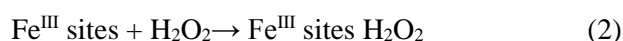


Fig. 5. Nitrogen adsorption/desorption isotherm and the corresponding pore size distribution curve of Fe₃O₄ NPs.

3.3. Degradation of MB dye

Here, the Fe₃O₄ NPs were utilized as a photocatalyst for MB degradation through a photo-Fenton reaction in the presence of H₂O₂ with visible light irradiation. In 1894, H.J.H. Fenton discovered the Fenton reaction, which involves the oxidation of organic and inorganic compounds in the presence of Fe²⁺ salts with H₂O₂ [31]. When the Fenton reaction was performed with UV, Visible, or solar light radiations, a large amount of •OH was generated compared to the Fenton or photolysis, which boosts the degradation of organic dyes [32, 33]. Mechanisms of the Fenton and photo-Fenton processes may be written as in equations (2) to (8) [32, 33] and **Scheme S1**.



Here, in the presence of H₂O₂, Fe³⁺ is reduced to Fe²⁺ with the generation of hydroperoxyl radicals (•O₂H). Then, the Fe²⁺ ions react with H₂O₂ to produce Fe³⁺ ions and are highly reactive •OH. In addition, the •OH was also generated upon the photolysis of H₂O₂. Furthermore, the MB dye reacts with •OH to form various degradation products. In the Fenton process, the reaction stops once all Fe²⁺ is consumed. However, in the presence of light, the reduction of Fe³⁺ regenerates Fe²⁺ (Eq. 8) [31, 33].

3.3.1. Effect of H₂O₂ dose

The effect of the H₂O₂ dose on the degradation of MB dye was carried out at different doses of H₂O₂, 0.07 to 0.5 mL, keeping MB concentration constant at 10 ppm and S:L ratio 0.05 g/L under the irradiation of visible light. **Fig. 6a** shows, the dose of H₂O₂ significantly affects the degradation of MB dye. As the dose of H₂O₂ increases from 0.07 mL to 0.5 mL, the degradation of MB dye increases from 95% to 100%, respectively, in about 35 min. In the case of 0.1 mL and 0.3 mL H₂O₂, the MB degradation achieved was 99% and 100% in about 40 min. At a lower dose of H₂O₂, 0.07 mL, the degradation was low compared to the high concentration

of H₂O₂, 0.5 mL. At lower concentrations, less amount of •OH has generated, which decreases the degradation rate. However, at a higher concentration sufficient amount of •OH was generated and complete degradation was attained in 35 min using 0.5 mL H₂O₂. Jiang et al. [10] have reported, a similar observation with Fe₃O₄ catalyst with H₂O₂ using a 10 ppm MB solution.

3.3.2. Effect of MB concentration

The effect of MB concentration was studied by varying the concentration of MB from 5 to 15 ppm at a constant dose of H₂O₂ (0.1 mL) and S:L ratio of 0.05 g/L, under visible light irradiation. As shown in **Fig. 7a**, as the MB concentration increases from 5 ppm to 15 ppm, the MB degradation decreased from 100% to 70%, respectively, in about 35 min. However, in the case of 10 ppm MB solution, the complete degradation was achieved in about 45 min. An increase in the concentration of MB augments the numbers of MB molecules on the surface of Fe₃O₄ NPs, whereas the amount of Fe₃O₄ NPs (i.e., active sites) and visible light intensity remain constant. In addition, as the MB concentration increases, the diffusion capacity of irradiated light decreases, which shut down the photo-Fenton reaction. Thus, as the MB concentration increases the generation of •OH decreases, which leads to less degradation of MB dye [19,34-36].

3.3.3. Effect of catalyst dosage

The effect of catalyst dosage on the degradation of MB dye was performed at different amounts of a catalyst such as 0.025, 0.05, and 0.075 g/L, keeping MB concentration and H₂O₂ dose constant at 10 ppm and 0.1 mL, respectively. It was observed that the rate and percentage of MB degradation were significantly affected by the catalyst dosage. As shown in **Fig. 8a**, as the catalyst dosage increases from 0.025 g/L to 0.075 g/L, the percentage of MB degradation decreased from 100% to 75%, respectively, in about 35 min. However, using 0.05 g/L catalyst dosage, complete degradation was achieved in about 45 min. It was observed that an increase in the catalyst dosage increases the turbidity, thus, the diffusion of irradiated light decreases, which reduces the generation of •OH and the photo-reduction of Fe³⁺ ions may slow down leading to less degradation. Harish et al. [37] and Patil et al. [18] have reported a similar observation with ZnO and α-Fe₂O₃ NPs. The increase in catalyst dosage above the optimum amount increases light scattering and significantly reduces the rate of reaction [38]. Moreover, as the catalyst dosage increases the suspended Fe₃O₄ NPs aggregate (particle-particles interactions) together, which results in a loss in

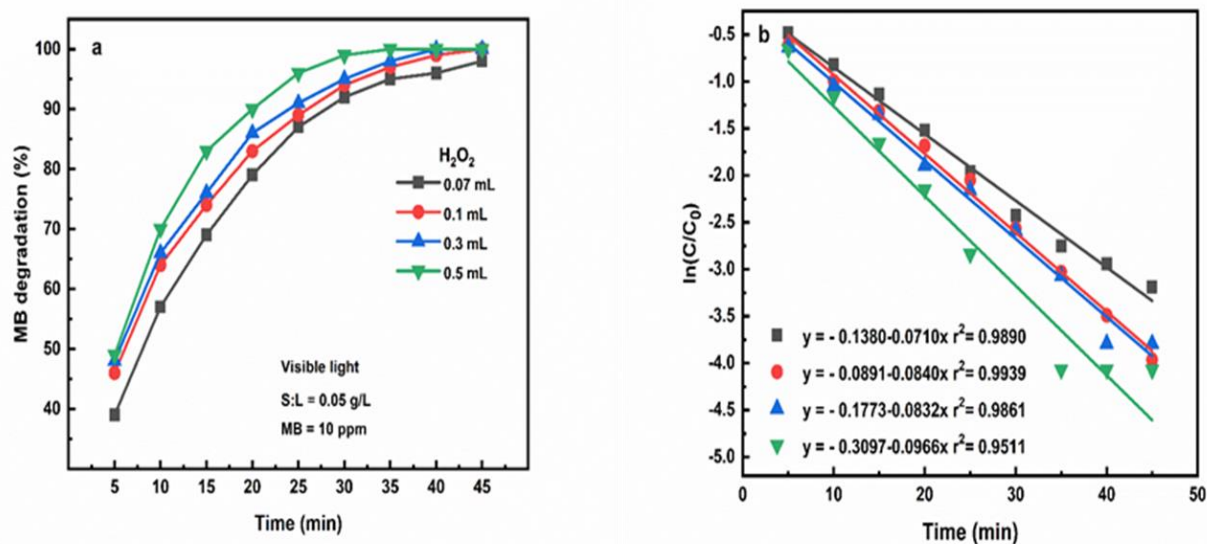


Fig. 6. a) Effect of H₂O₂ dose on the MB degradation, and b) Typical Hinshelwood plots of ln(C/C₀) vs time at different H₂O₂ doses (reaction conditions: S:L = 0.05 g/L, MB = 10 ppm, under visible light).

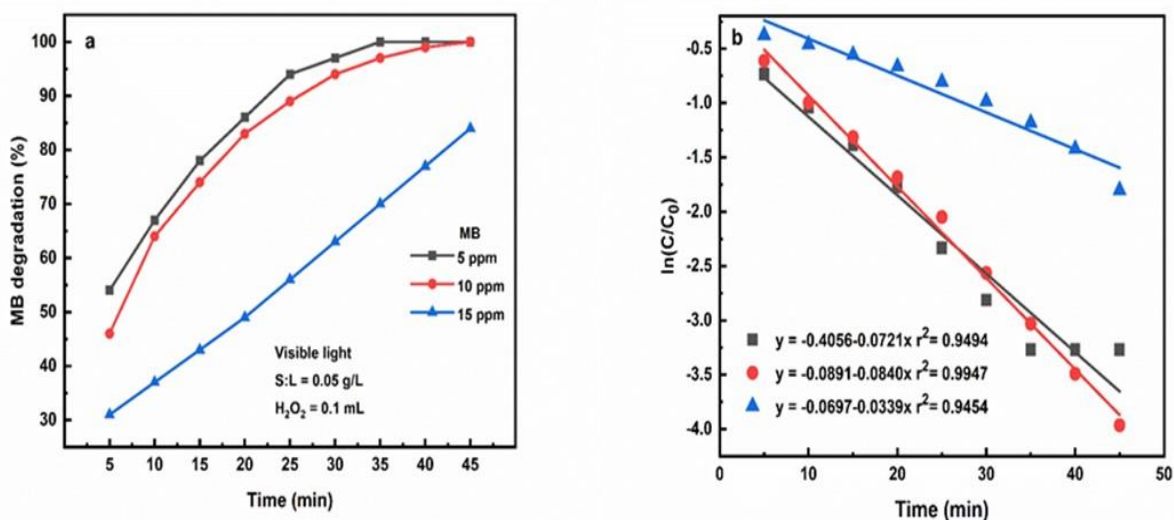
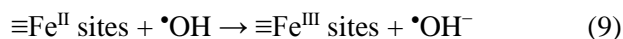


Fig. 7. a) Effect of dye concentration on the MB degradation and b) Typical Hinshelwood plots of ln(C/C₀) vs time at various dye concentrations (reaction conditions: S:L = 0.05 g/L, H₂O₂ dose = 0.1 mL under visible light).

surface area and reduces the amount of irradiated light reaching the active site of NPs and subsequently, decreases the rate of reaction [38-40]. On the other hand, according to Ahmed et al. [33], the decrease in degradation is due to the scavenging effect of $\bullet\text{OH}$ during unwanted side reactions (Eq. 9).



In addition, two individual MB degradation experiments were carried out without H₂O₂ and in the absence of a

catalyst (**Fig. 9a**). In the case of the absence of H₂O₂ the 10 ppm MB degradation was carried out with 0.05 g catalyst alone and it was observed that the degradation was about 12%. However, in the case of the absence of a catalyst with 0.1 mL H₂O₂, 22% of degradation was achieved in about 45 min. Similar observations were reported by Liu et al. [12], Patil et al. [18], and Gupta et al. [41]. From the above observations, it was clear that alone H₂O₂ and catalyst do not bring a significant degradation of MB dye. On the other hand, the Fe₃O₄

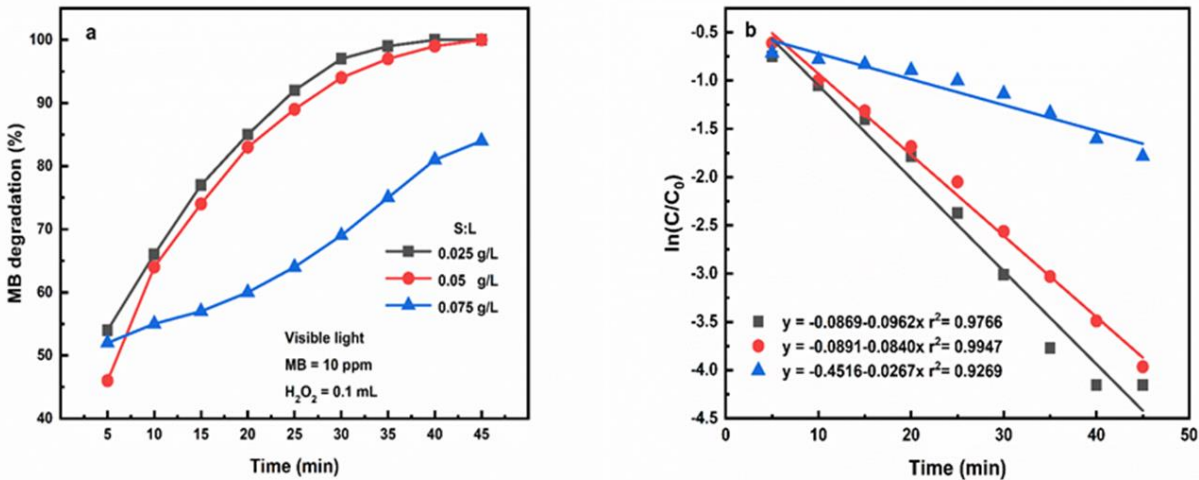


Fig. 8. a) Effect of catalyst dosage on the MB degradation, and b) Typical Hinshelwood plots of $\ln(C/C_0)$ vs time at different S:L ratio (reaction conditions: MB = 10 ppm, H₂O₂ dose = 0.1 mL under visible light).

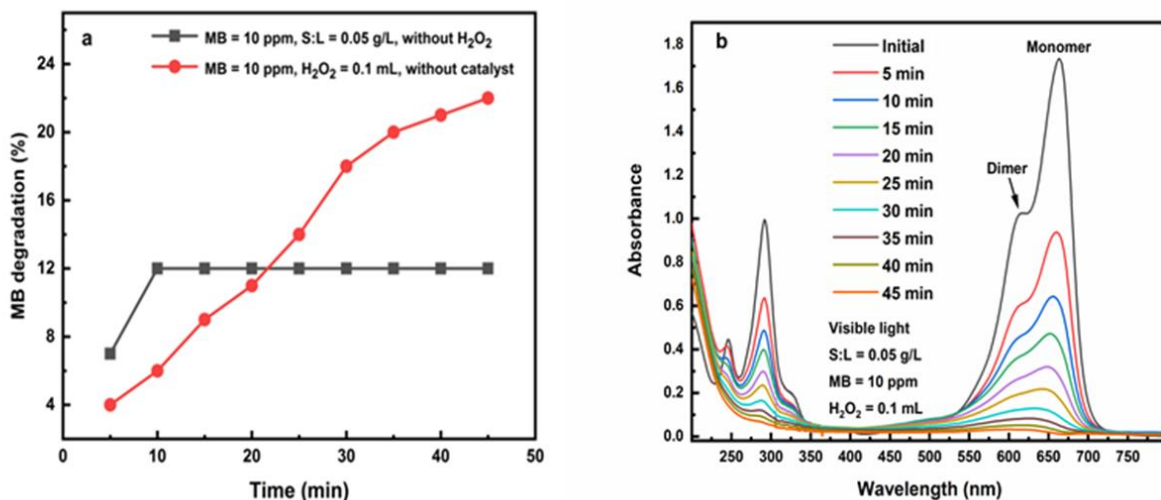


Fig. 9. a) MB degradation without H₂O₂ (reaction conditions: MB = 10 ppm, S:L = 0.05 g/L), without catalyst (reaction conditions: MB = 10 ppm, H₂O₂ dose = 0.1 mL) under visible light, and b) Time-dependent UV-Vis spectra of MB during degradation in a typical case (reaction conditions: MB = 10 ppm, S:L = 0.05 g/L, H₂O₂ dose = 0.1 mL under visible light).

NPs show complete degradation in the presence of H₂O₂.

From the above experimental results, the optimum conditions for the degradation of MB were summarized as 10 ppm MB solution, 0.1 mL H₂O₂, and 0.05 g/L S:L ratio under visible light irradiation. Figure 9b shows the time-dependent UV-Vis spectra of MB during the degradation process at the optimum conditions, wherein the absorption maximum peak at $\lambda_{\max} = 664$ nm and $\lambda_{\max} = 290$ nm steadily declines and disappeared at 45 min. The absorption peak at 664 nm corresponds to the monomer of free MB and a peak at 610 nm is from the

H-dimer in water solution [42]. On the other hand, the trimer state of MB is found at 570 nm [42], which is not observed in this study.

3.3.4. Kinetics study of MB degradation

The degradation of MB dye takes place on the surface of the Fe₃O₄ catalyst. On the surface of the catalyst, reactive species such as e/h pairs, hydroxyl, and superoxide radicals were produced. These species have a very short lifetime of about a few nanoseconds and are responsible for degradation, which is correlated to the rate constant. In an equilibrium degradation process, the

kinetic of the MB degradation reaction can be interpreted using the Langmuir–Hinshelwood equation (10), which assumes that both species are present in a monolayer at the solid-liquid interface to control the rate of the process. The Langmuir–Hinshelwood equation (10) can be modified into a logarithmic form equation (11) upon integration of equation (10), which is similar to an apparent pseudo-first-order equation [43-45].

$$r = -dC/dt = (k'KC)/(1 + KC) = k'\theta \quad (10)$$

$$\ln(C_o/C) + k'(C_o - C_t) = k'Kt = kt \quad (11)$$

Where k' is the specific reaction rate constant in mg/L min, K represents the equilibrium constant of the reactant in L/mg, C is the concentration of dye, t is irradiation time, and k shows the apparent first-order rate constant. At the concentration of dye > 5 mM, the reaction is zero-order kinetics, whereas at a lower concentration (< 1 mM) the reaction is first-order kinetic [43-45]. In the case of H_2O_2 dosage (Figure 6b), the rate constants were 0.071, 0.084, 0.083, and 0.096 min^{-1} at 0.07, 0.1, 0.3, and 0.5 mL H_2O_2 dosage, respectively. However, in the case of MB concentration (Figure 7b), the rate constant observed was 0.072, 0.084, and 0.033 min^{-1} at 5, 10, and 15 ppm MB, respectively. The rate constant decreases from 0.096, 0.084, and 0.026 min^{-1} as the catalyst dosage increased from 0.025, 0.05, and 0.075 g/L, respectively (Fig. 8b). At optimum

conditions, the rate constant for the MB degradation process is 0.084 min^{-1} . The results clearly show that the MB degradation follows pseudo-first-order kinetics.

To understand the mechanism of MB degradation in the presence of Fe_3O_4 NPs and H_2O_2 . The active species scavenger experiments were performed at optimum conditions such as 10 ppm MB solution, 0.1 mL H_2O_2 , and 0.05 g/L S:L ratio under visible light irradiation. Here, ethylenediamine tetraacetic acid disodium salt (Na_2EDTA , 3 mM), p-benzoquinone (BQ, 3 mM), and isopropyl alcohol (IPA, 3 mM) were used as a reactive scavenger to trap the hole (h^+), superoxide ($O_2^{\cdot-}$) and hydroxyl (OH^{\cdot}) radicals, respectively [36]. As shown in Fig. 10, in the presence of Na_2EDTA and BQ the MB degradation was 93% and 87%, respectively, which confirms that the h^+ and $O_2^{\cdot-}$ radicals have a negligible role in the degradation. However, in the presence of IPA, the degradation was only 15%, this implied that the generated OH^{\cdot} radical play an important role in the MB degradation. Liu et al. [12] and Gupta et al. [41] have reported similar observations with $\alpha-Fe_2O_3$ NPs and MFe_2O_4 NPs in the presence of H_2O_2 . Nezamzadeh-Ejhi et al. [27], have reported the GC-MS data, which shows phenol, N,N' -dimethylbenzene-1, 4-diamine, N -(3, 4-dihydroxy phenyl)- N -methyl formamide, 4-aminobenzene-1, 2-diol, and 2-amino-5-(N -methyl formamide) benzene sulfonic acid was an intermediate compound formed during MB degradation.

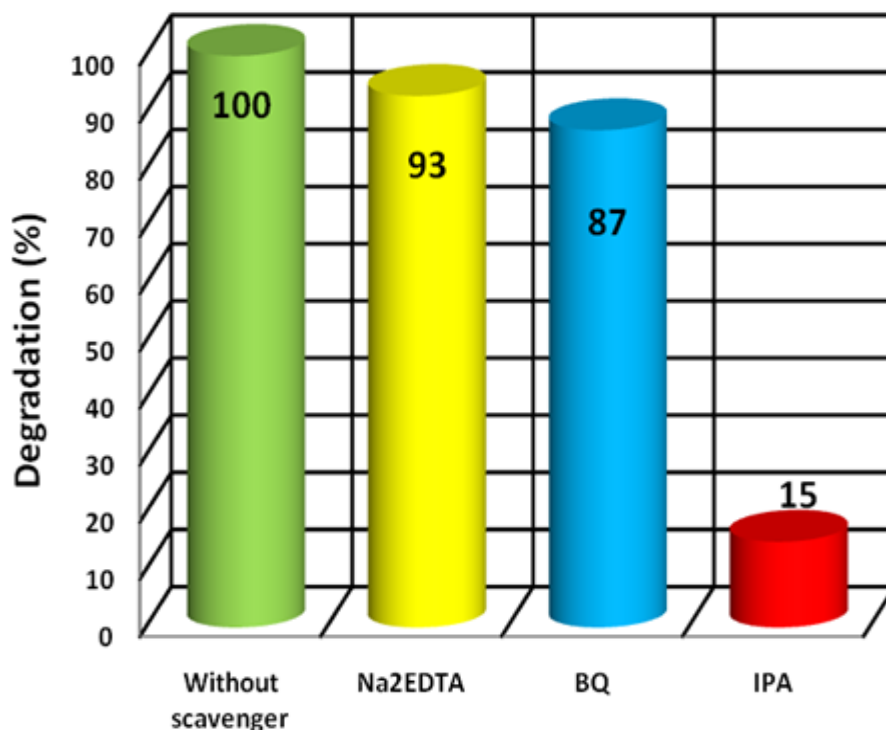


Fig. 10. Effect of reactive scavengers Na_2EDTA (3 mM), BQ (3mM), and IPA (3mM) on the photodegradation of MB dye under visible light (reaction conditions: MB = 10 ppm, S:L = 0.05 g/L, H_2O_2 dose = 0.1 mL).

4. Conclusions

In this study, the dissolution of soft magnetic FeSiAl alloy cores of spent PCBs was carried out successfully using a mixture of mild organic acids, CA, and AA. The dissolved Fe was selectively precipitated as Fe₃O₄. The obtained Fe₃O₄ NPs were utilized for the degradation of methylene blue dye in the presence of H₂O₂ under visible light. The kinetic calculation of the MB degradation process was performed using Langmuir–Hinshelwood model, which shows that the reactions follow pseudo-first-order kinetics. The active species scavenger experiments confirm the OH[•] radical play an important role in MB degradation.

Acknowledgements

Authors gratefully acknowledge the funding received from VGST-CESEM (KSTePS/VGST/CESEM/2018-19/GRD No. 746), Govt. of Karnataka.

Conflict of interest

The authors declare that they have no known competing financial interests or personal relationships that could have appeared to influence the work reported in this paper.

References

[1] F. Fiorillo, G. Bertotti, C. Appino, M. Pasquale, (1999).

[2] Y. Guo, J. Zhu, H. Lu, Z. Lin, Y. Li, IEEE Trans. Magn. 48 (2012) 3112–3115.

[3] H. Shokrollahi, K. Janghorban, J. Mater. Process. Technol. 189(1) (2007) 1-12.

[4] D. Mmereki, B. Li, A. Baldwin, L. Hong, E-waste transit.-from Pollut. to Resour. 2016.

[5] M. Farrokhi, S-C. Hosseini, J-K. Yang, S-S. Mehdi, Water Air Soil. Pollut. 225 (2014) 2113.

[6] N. Jaafarzadeh, A. Takdastan, S. Jorfi, F. Ghanbari, M. Ahmadi, G. Barzegar, J. Mol. Liq. 256 (2018) 462-470.

[7] E.S. Ngankam, D-Y. Lemankreo, B. Debina, A. Baçaoui, A. Yaacoubi, A.N. Rahman, Mater. Sci. appl. 11 (2020) 382-400.

[8] ReportLinker. Global textile dyes industry. Globe Newswire (2020). <https://www.reportlinker.com/p05151463/?utm>.

[9] Fibre2Fashion. Booming textile dyes industry in emerging economies. F2F NewsLetter (2014). doi:<https://www.fibre2fashion.com/industry->

article/7422/booming-textile-dyes-industry-in-emerging-economies

[10] J. Jiang, J. Zou, L. Zhu, L. Huang, H. Jiang, Y. Zhang, J. Nanosci. Nanotechnol. 11(6), (2011) 4793-4799.

[11] R. Vijayan, S. Joseph, B. Mathew, Bio. Nano. Sci. 8 (2018) 105–117.

[12] J. Liu, B. Wang, Z. Li, Z. Wu, K. Zhu, J. Zhuang, Q. Xi, Y. Hou, J. Chen, M. Cong, J. Li, G. Qian, Z. Lin, J. Alloys Compd. 771 (2019) 398–405.

[13] S. Xing, Z. Zhou, Z. Ma, Y. Wu, Appl. Catal. B 107 (2011) 386–392.

[14] G. Xie, P. Xi, H. Liu, F. Chen, L. Huang, Y. Shi, F. Hou, Z. Zeng, C. Shaob, J. Wang, J. Mater. Chem. 22 (2012) 1033-1039.

[15] Q. Wu, C. Feng, C. Wang, Z. Wang, Colloids Surf. B, 101 (2013) 210–214.

[16] Z. Wang, Y. Fan, R. Wu, Y. Huo, H. Wu, F. Wang, X. Xu, RSC Adv., 8 (2018) 5180-5188.

[17] H. Sun, L. Cao, L. Lu, Nano. Res., 4(6) (2011) 550–562.

[18] M.N. Pervez, W. He, T. Zarra, V. Naddeo, Y. Zhao, Water, 12(3) (2020) 733.

[19] D. Patil, M.B. Sridhara, J. Manjanna, G.P. Nayaka, S. Sabale, Ceram. Int., 48(23) (2022) 35848-35859.

[20] J. Basset, R.C. Denny, G.H. Jeffery, J. Mendham, “Vogel's textbook of quantitative inorganic analysis”, fourth ed. ELBS/Longman, London (1978).

[21] L. Huang, X. Liu, D. Chuai, Y. Chen, R. Yu, Sci. Rep., 6 (1) (2016) 35377.

[22] Z. Hou, P. Yan, B. Sun, H. Elshekh, B. Yan, Results Phys., 14 (2019) 102498.

[23] Y. Janu, D. Chaudhary, V. Chauhan, L. Saini, M.K. Patra, SN Appl. Sci., 2 (2020) 2–10.

[24] F. Azadi, A. Jashni, M.M. Zerafat, Ecotoxicol. Environ. Saf., 165 (15) (2018) 467-475.

[25] Y.P. Yew, K. Shameli, M. Miyake, N. Kuwano, N.B. Bt Ahmad Khairudin, S.E. Bt Mohamad, K.X. Lee, Nanoscale Res. Lett., 11 (2016) 276.

[26] S.R. Kumar, M. Paulpandi, M. Manivelraja, D. Mangalaraj, C. Viswanathan, S. Kannan, N. Ponpandian, RSC Adv., 4 (2014) 13409-13418.

[27] A. Nezamzadeh-Ejhi, M. Karimi-Shamsabadi, Appl. Catal. A Gen. 477 (2014) 83–92.

- [28] M. Balakrishnan, R. John, *Iran. J. Catal.* 10(1) (2020) 1-16.
- [29] M. Zebardast, A.F. Shojaei, K. Tabatabaeian, *Iran. J. Catal.* 8(4) (2018) 297-309.
- [30] S. Zhang, W. Wu, X. Xiao, J. Zhou, F. Ren, C. Jiang, *Nanoscale Res. Lett.*, 6 (2011) 89.
- [31] A. Babuponnusami, K. Muthukumar, *J. Environ. Chem. Eng.*, 2 (2014) 557–572.
- [32] X. Yang, W. Chen, J. Huang, Y. Zhou, Y. Zhu, C. Li, *Sci. Rep.*, 5 (2015) 10632.
- [33] Y. Ahmed, Z. Yaakob, P. Akhtar, *Catal. Sci. Technol.*, 6(1) (2016) 222–1232.
- [34] D. Suresh, Udayabhanu, P.C. Nethravathi, K. Lingaraju, H. Rajanaika, S.C. Sharma, H. Nagabhushana, *Spectrochim. Acta A*, 136 (2015) 1467-1474, 2015.
- [35] C. Anupama, A. Kaphle, Udayabhanu, G. Nagaraju, *J. Mater. Sci. Mater. Electron*, 29, (2018) 4238-4249.
- [36] D. Patil, J. Manjanna, S. Chikkamath, V. Upper, M. Chougala, *J. Hazard. Mater. Adv.* 4 (2021) 100032.
- [37] S. Harish, M. Navaneethan, J. Archana, A. Silambarasan, S. Ponnusamy, C. Muthamizhchelvan, Y. Hayakawa, *Dalt. Trans.* 44 (2015) 10490–10498.
- [38] A. Pourtaheri, A. Nezamzadeh-Ejhieh, *Spectrochim. Acta A Mol.* 137 (2015) 338–344.
- [39] K.M. Reza, A.S.W Kurny, F. Gulshan *Appl. Water Sci.* 7 (2017) 1569–1578.
- [40] F.A. Aisien, N.A. Amenaghawon, E.F. Ekpenisi, *J. Eng. Appl. Sci.* 9 (2013) 11-16.
- [41] N.K. Gupta, Y. Ghaffari, S. Kim, J. Bae, K.S. Kim, Md. Saifuddin, *Sci. Rep.* 10 (2020) 4942.
- [42] B. Liu, L. Wen, K. Nakata, X. Zhao, S. Liu, T. Ochiai, T. Murakami, A. Fujishima, *Chem. Eur. J.* 18(40) (2012) 12705-12711.
- [43] B. Manikandana, K.R. Muralib, R. Johna, *Iran. J. Catal.* 11(1) (2021) 1-11.
- [44] M. Mehrali-Afjani, A. Nezamzadeh-Ejhieh, H. Aghaei, *Chem. Phys. Lett.* 759 (2020) 137873.
- [45] A. Yousefi, A. Nezamzadeh-Ejhieh, *Iran. J. Catal.* 11(3), (2021), 247-259.